Describing function analysis of limit cycle in a multiple flame combustor

Jomaas, Grunde

Published in:
Proceedings of the gas turbine technical congress and exposition

Publication date:
2010

Document Version
Early version, also known as pre-print

Proceedings of ASME Turbo Expo 2010: Power for Land, Sea and Air
GT2010
June 14-18, 2010, Glasgow, UK

GT2010-22372

DRAFT : DESCRIBING FUNCTION ANALYSIS OF LIMIT CYCLES IN A MULTIPLE FLAME COMBUSTOR

Frédéric Boudy*, Daniel Durox, Thierry Schuller, Grunde Jomaas†, Sébastien Candel‡
Laboratoire EM2C - Ecole Centrale Paris - CNRS
Grande voie des vignes, 92295 Châtenay-Malabry, France
Email: frederic.boudy@em2c.ecp.fr

ABSTRACT

A recently developed nonlinear Flame Describing Function (FDF) is used to analyze combustion instabilities in a system where the feeding manifold has a variable size and where the flame is confined by quartz tubes of variable length. Self-sustained combustion oscillations are observed when the geometry is changed. Regimes of oscillation are characterized at the limit cycle and also during the onset of oscillations. Theoretical predictions of the oscillation frequencies and levels are obtained using the FDF. This generalizes the concept of flame transfer function by including a dependence on the frequency and on the level of oscillation. Predictions are compared with experimental results for two different lengths of the confinement tube. These results are in turn used to predict most of the experimentally observed phenomena and in particular the correct oscillation levels and frequencies at limit cycles.

INTRODUCTION

Reduction of pollutant emissions to meet environmental regulations has led to novel solutions in combustor design. Advanced systems use new premixed burners in which the flame is more compact. The amount of cooling air supplied through the chamber walls is reduced and acoustic damping by the cooling liner is diminished. As these systems operate near the blow-out limit, the flame is more sensitive to equivalence ratio and flow rate fluctuations. These conditions give rise to combustion instabilities in which the flame dynamics is coupled to the acoustic resonant modes of the system. Conditions inducing such instabilities were recognized more than hundred years ago [1] and a considerable amount of research has been devoted to the many issues raised by these phenomena (see for example [2, 3] for classical monographies and [4–6] for some recent reviews). Progress has been substantial, but research is still needed to develop predictive methods for instabilities and design instability free combustors.

While the acoustic features of the problem are now well documented and can be determined with linearized solvers and their nonlinear extensions, the coupling between acoustics and combustion and the resulting flame dynamics are more complex. The modeling of the flame dynamics constitutes a central challenge in this field. This aspect was treated in the early investigations of rocket engine instabilities by introducing a gain and a delay in the response of combustion to pressure perturbations (see for example [2]). In the $n-\tau$ modelling developed in the early period of rocket propulsion the amplitude and timing of the combustion response is represented by an interaction index n and a delay τ. This attractively simple model has been widely used but tends to hide the physics driving the process. As a result, many of the more recent studies have tried to capture the combustion response for example by determining the frequency dependence in terms of a flame transfer function (FTF). This can be used to define the sensitivity of the flame to external perturbations and see if the combustion process is able to add energy to one of the acoustic modes of the system. It also indicates if the energy is transferred at the right phase of the pressure oscillation. FTFs can be obtained experimentally [7–10], theoretically [7, 11–13] or numerically [14–18]. These studies indicate that the delay in

*Address all correspondence to this author.
†Currently at Technical University of Denmark (DTU)
‡Also with Institut Universitaire de France

the flame response is associated to the convection time of flow perturbations.

Flame transfer functions are now used to predict stability maps of various types of systems, by combining descriptions of the acoustic field with the combustion response [19–21]. This is illustrated in the case of a gas turbine combustor operating at atmospheric pressure [22] where the phase corresponds to a delay τ and the gain is measured with a dual microphone technique. Acoustic calculations yield a rough stability map for the system. Acoustic transfer matrices are extensively used to model the chamber response [23] offering a natural framework for experimentally determined flame transfer functions describe the combustion response to downstream and upstream disturbances. This approach is well illustrated in a recent investigation of a swirled V-flame response [24]. Experimental results are used to define a theoretical FTF with a gain represented by a second order low pass filter. This is used in a second step to predict longitudinal self-sustained acoustic oscillations. The linear analysis indicates that the system will oscillate on the first mode, but does not provide the limit cycle amplitude observed experimentally. Transfer functions have been measured under high pressure conditions of a real burner [25]. These data were then used to estimate the instability frequencies of a high pressure gas turbine equipped with an annular combustor and it was possible to predict the instability frequencies of the system under operating conditions. Numerical simulations of self-sustained oscillations [26] developed in the case of an aero-engine combustor are used to obtain the interaction index n and time delay τ of the process. This information combined with a Helmholtz solver is then used to provide a linear description of the process.

Linear modeling has been widely used but its results are limited. In this framework it is not possible to predict many phenomena observed in practice, such as frequency shifting during transient growth of oscillations, mode switching, instability triggering or hysteresis and the limit cycle amplitudes cannot be inferred. To account for these observations and determine limit cycle levels of oscillation one has to represent the nonlinear response of the flame. This is demonstrated by Dowling [27] in an analysis of a ducted V-flame response to incident disturbances. The nonlinear saturated response of the flame results in this case from the motion of the flame anchor point and it is represented by a describing function. This work was later extended [28] by introducing a time lag model including an imposed level of saturation with respect to the perturbation amplitude. It is concluded by Lieuwen and Bellows [29] that the response saturation led to a state where the flame could not provide enough energy to overcome the damping of the system. This is supported by measurements of swirled flame dynamics [30] showing the influence of fluctuation amplitudes on saturations and nonlinearities. Balachandran et al. [31] find that nonlinearities appear when the relative level of fluctuation exceeds 15% in the case of a V-flame. The results are explained in terms of the flame front kinematics, which plays a major role in the saturation mechanism. Durox et al. [9, 32] indicate that the initial flame geometry has a major influence on the nonlinear response of flames to incident disturbances. In certain cases, the nonlinear behavior can be obtained even for relatively small amplitudes. Depending on the geometry, nonlinearities influence the gain or the phase between the perturbations and the heat release rate fluctuations [9, 24, 33, 34].

The unified framework for instability analysis developed by Noiray et al. [35] relies on the flame describing function (FDF) concept. The flame response is represented by transfer functions which depend on frequency *and* on the level of incident perturbations. The describing function is then formed by a family of amplitude dependent transfer functions. The FDF of a collection of unconfined flames anchored on a multipoint injector was measured in a systematic fashion. Using these data, it was possible to develop a nonlinear dispersion relation, deduce growth rates depending on the incident disturbance amplitude and explain phenomena such as hysteresis, nonlinear instability triggering, and mode switching with excellent comparisons with experimental observations. The work was extended to confined configurations [36] but without experimental comparisons. An amplitude dependent n-τ [37] is used to represent limit cycle oscillations of a ducted V-flame. Using experimental data, the time lag τ is made to change with the oscillation level and the interaction index is represented by a second order low pass filter shape. This model only partially retrieves experimental observations. Numerical calculations [38] indicate that self-sustained oscillations can be simulated in fairly complex geometries (in this case with an annular combustor), but the required computational resources do not allow a fast exploration of the useful parameter space.

The present work focuses on the prediction of combustion instabilities using the FDF framework. This is applied to a generic configuration comprising a feeding manifold, an injection and flame anchoring system and a confinement tube. Emphasis will be put on the prediction of oscillation limit cycle levels and frequencies as a function of modifications of the burner geometry. After a description of the experimental setup, instabilities will be characterized for different system geometries. Following that, a theoretical model will be developed to predict the different unstable regimes and results will be compared to systematic experiments.

1 Experimental setup and combustion regimes

The experimental setup is sketched in Fig. 1. The three main elements of the burner are the feeding manifold, a perforated plate which delivers the premixed streams and anchors the flames and the quartz confinement tube. The combustion zone is placed in this quartz tube. The reactants are premixed in the piston before they are injected into the enclosing manifold. The piston also facilitates changes in the length of the feeding manifold. The perforated plate, which is confined within a quartz tube

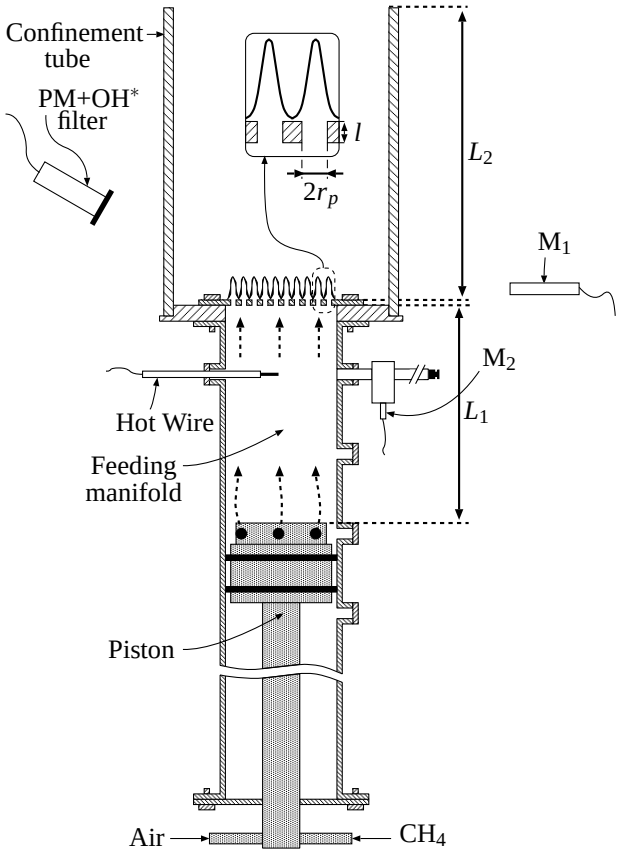

Figure 1. Experimental setup used to characterize self-sustained instabilities.

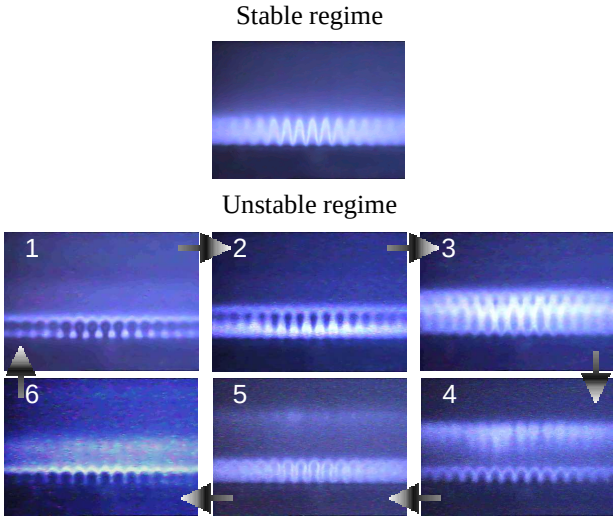

Figure 2. Stable and unstable combustion regimes at 750 Hz for an equivalence ratio ϕ=1.03.

at the top of the feeding manifold, anchors an ensemble of small laminar conical flames. It has a thickness of l=3 mm and a diameter of $2R$=70 mm, is made of stainless steel, and comprises N=420 holes of diameter $2r_p$=2 mm placed on a 3 mm square mesh, resulting in a global porosity $\mathcal{P} = N\pi r_p^2/\pi R^2$ of 0.34. Four quantities are measured in this experiment. The fluid velocity in the feeding manifold is determined with a hot wire probe 3 cm below the perforated plate. A photomultiplier equipped with an OH^* filter (λ=308 nm) views the flames from outside the confinement and provides a signal almost proportional to the heat release rate [39]. The pressure fluctuations are measured inside the feeding manifold with the microphone M_2 placed in a waveguide in front of the hot wire and another microphone M_1 outside the confinement tube 24.5 cm away from the burner axis detects the radiated sound pressure level. The length of the feeding manifold, as measured between the upstream side of the perforated plate and the head of the piston, can be varied in discrete steps all the way from L_1=0.15 m to 0.54 m. The piston head is designed to offer a quasi-perfect reflecting boundary for acoustic waves. Two lengths of confinement tubes are used in the present study. In the first case, the length of the feeding manifold is swept with a confinement tube L_2=0.1 m. Then, another tube L_2=0.2 m is used in a second set of exploration. The flow rate of the methane/air premixture is $\dot{m}$=4.71$\times 10^{-3}$ kg/s at an equivalence ratio ϕ=1.03, providing a thermal power of 13.3 kW. For both confinement tubes, the system is unstable for a wide range of feeding manifold lengths (L_1) and only stable for some. In a stable case, as shown in Fig. 2, flames have a conical shape. In the unstable cases, all the flames move in a regular fashion with formation and collapse of fresh reactant pockets as illustrated in Fig. 2. This behavior causes a strong level of noise, which can exceed 110 dB on the microphone M_1 (with a reference pressure 2×10^{-5} Pa). The experimental procedure is initiated with the head of the piston L_1=0.15 m away from the perforated plate (minimum extension) and consists of acquiring the sensor signals at limit cycles. Then, the piston is retracted in increments of one centimeter all the way to a manifold length L_1=0.54 cm (maximum extension) with signals being acquired for each step. The piston is then moved in the reverse direction (maximum to minimum extension) using the same increment and acquiring the same set of signals. As a result, the oscillation frequencies and the amplitudes of pressure oscillations are obtained for a range of manifold lengths. These experiments are repeated for the two flame confinement tubes L_2=0.1 m and 0.2 m.

Another set of experiments is conducted to get the response of the flame ensemble to velocity fluctuations i.e. the FDF of the flames [35]. This system, shown in Fig. 3, allows measurements of heat release rate fluctuations through the values of the light emission fluctuations of the OH^* radical acquired by a photomultiplier (PM). Velocity fluctuations are obtained from LDV (Laser Doppler Velocimetry) measurements inside one flame 0.7

mm above the hole.

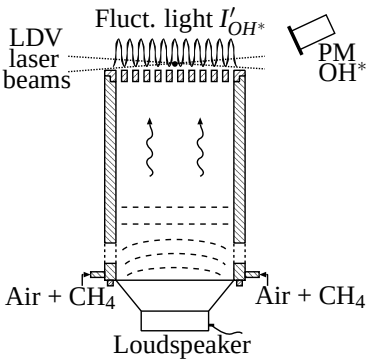

Figure 3. Forced flow setup used to determine the FDF. The forced flow fluctuations are created by a loudspeaker placed at the bottom of the burner. Velocity fluctuations are measured by LDV at the base of one flame, 0.7 mm above the hole and heat release rate fluctuations are deduced from I'_{OH^*} measured by the photomultiplier.

2 Experimental results

The first set of data correspond to the L_2=0.1 m flame confinement tube. Figure 4 illustrates the evolution of frequency and pressure for different lengths of feeding manifold. The dashed lines represent the acoustic eigenmodes evolution for a variable feeding manifold length L_1. For a range, between L_1=0.23 m and 0.27 m, the system is stable and the pressure measured by microphone M_2 falls under 120 dB which is the noise level corresponding to that of the flow and combustion alone. Sound pressure level, 24.5 cm away from the center of the burner (M_1), reaches 120 dB for the unstable regimes and 95 dB in the stable cases. It is noteworthy that the frequency evolves differently for the two directions of piston movement (min to max vs. max to min). In the first movement sequence (min to max) the frequency evolves around the first mode (L_1=0.15 m to 0.22 m), reaches a stable band, and then switches to the second mode (L_1=0.27 m to 0.54 m). In the reverse direction (max to min) the frequency remains on the second mode between L_1=0.54 m to 0.26 m, as it should, reaches a stable band, and then continues on the second mode from L_1=0.22 to 0.18 m before finally switching to the first mode for L_1=0.17 m to 0.15 m. Therefore, it is established that the instabilities present an hysteresis in this confinement case. In a second set of experiments, the flame confinement tube was changed to one of L_2=0.2 m. The evolution of oscillation frequency and pressure level is presented in Fig. 5. The stable zone still appears in this configuration but its appearance is delayed until the length of the manifold reaches L_1=0.26 m and the system remains stable

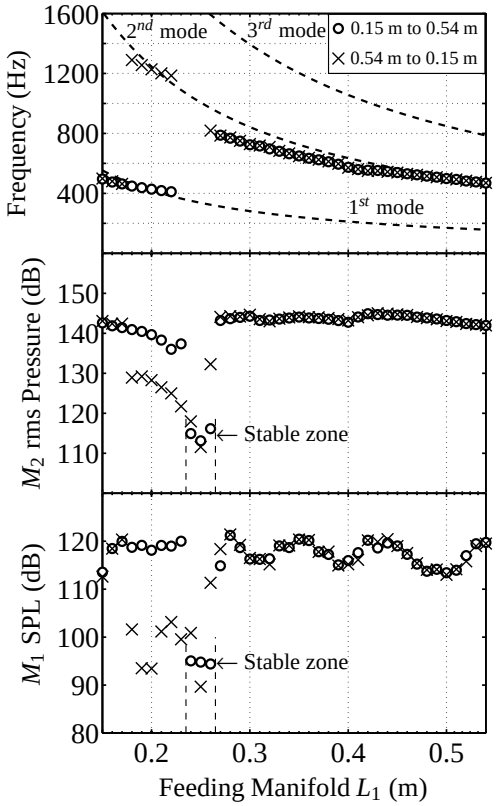

Figure 4. Frequency and pressure level evolution with the L_2=0.1 m confinement tube, swept from 0.15 m to 0.54 m (o) and from 0.54 m to 0.15 m (x) of feeding manifold. The acoustic eigenmodes without combustion are plotted with dashed lines.

until L_1=0.30 m. Thus, the change of the downstream confinement length has altered the system stability. For the short manifold lengths L_1=0.15 m to 0.25 m, the frequency evolution still closely matches the first mode, and after the stable zone, the second mode is seen for L_1=0.31 m to 0.54 m. The reverse evolution of the piston gives the same set of data, which indicates that there is no hysteresis for this confinement length L_2=0.2 m. This type of features, like the oscillation level and hysteresis phenomena cannot be anticipated using classical linear stability analysis and these data can be used to validate the FDF methodology.

3 Nonlinear analysis

A nonlinear analytical model is needed to capture the rich physics behind the observed phenomena. In addition, such a model will be of value for predicting and understanding mechanisms of frequency switching or hysteresis in this system. In the following analysis, fluctuating quantities are written as a sum of a mean quantity and a fluctuation : $a = \bar{a} + a'$. The analysis is carried out in the frequency domain and each fluctuating quan-

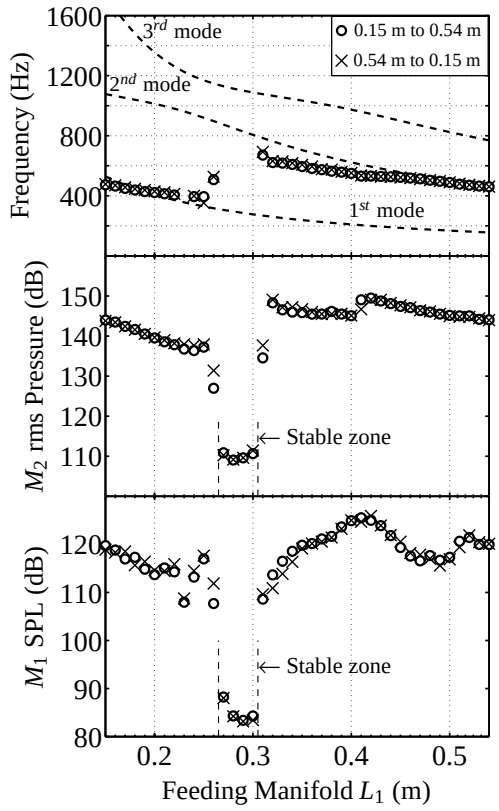

Figure 5. Frequency and pressure level evolution with the L_2=0.2 m confinement tube, swept from 0.15 m to 0.54 m (o) and from 0.54 m to 0.15 m (x) of the feeding manifold. The acoustic eigenmodes without combustion are plotted with dashed lines.

tity takes the form : $a' = |a'|e^{-i\omega t}$ where $\omega = \omega_r + i\omega_i$, ω_r corresponds to the angular frequency ($2\pi f$) and ω_i is the growth rate. A perturbation grows for positive values of growth rate while it decays for negative ones. The analytical work performed here follows that developed previously [36] where a dispersion relation is derived and combined with the FDF to analyse the dynamics of a confined system. Given the low unstable frequencies observed in the experiments, the wavelengths are long compared to the dimensions of the system to consider other acoustic waves than longitudinal ones. The flame is thus compact. The different elements of the system are modeled as an acoustic network. The influence of the flames is taken into account in the matching condition between the feeding manifold and the confinement tube through the expansion of gases. This method has already been used to analyze thermo-acoustic coupling phenomena (see for example [20, 40, 41]). The burner is modeled as illustrated in Fig. 6. In each tube section, temperature, density, velocity and pressure are all subscripted with their respective numbers and mean quantities ($\overline{T}, \overline{\rho}$) are considered uniform. The pressure and

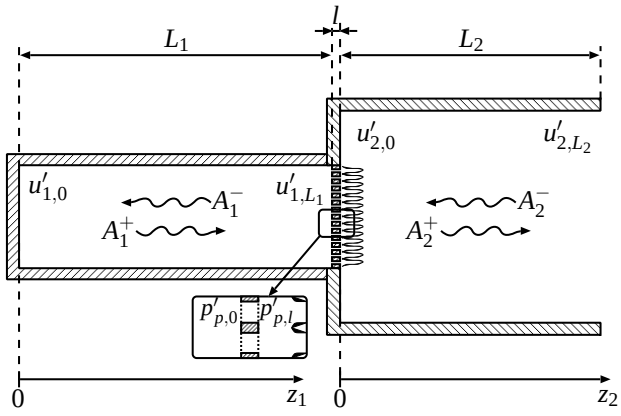

Figure 6. Burner and symbol convention used for the analytical model.

the velocity fluctuations are written as follows for the n^{th} tube :

$$u'_{n,z_n} = \frac{1}{\rho_n c_n}\left(A_n^+ e^{ik_n z_n} - A_n^- e^{-ik_n z_n}\right)$$
$$p'_{n,z_n} = A_n^+ e^{ik_n z_n} + A_n^- e^{-ik_n z_n} \quad (1)$$

where z_n stands for the position, k_n the wave number ($k_n = \omega/c_n$) and c_n the speed of sound which differs in the premixer c_1=340 m/s and the flame tube c_2=850 m/s. These relations are completed by matching and boundary conditions. The head of the piston offers a quasi-perfect reflecting boundary condition which gives $u'_{1,0}$ = 0. At the combustor outlet the pressure fluctuation vanishes and yields p'_{2,L_2} = 0. In this model, no end correction is taken into account, but it would be easy to include as all it does is to augment the length of the confinement tube by a factor of 0.85 times the radius. The perforated plate is considered with bulk oscillations of velocity in the apertures. Based on Melling's work [42], Noiray et al. [35] derived a relation that links the pressure between the upstream and downstream sides of the perforated plate :

$$p'_{p,l} - p'_{p,0} = i\omega\rho_1 l\left(1 + \frac{l_\nu}{r_p}(1+i)\right)u'_p \quad (2)$$

where $l_\nu = (2\nu/\omega)^{1/2}$ stands for the viscous acoustic boundary layer thickness and ν the kinematic viscosity. Each side of the perforated plate is linked with the upstream or the dowstream cavity where the following relations are satisfied :

$$p'_{p,0} = p'_{1,L_1}\,, \quad p'_{p,l} = p'_{2,0}\,, \quad S_1 u'_{1,L_1} = N S_p u'_p \quad (3)$$

where S_1 is the surface area of the feeding manifold section, S_p the surface area of one aperture and N the number of holes. Com-

bining (Eq. 2) and (Eq. 3) it is possible to find the pressure jump condition between the upstream and downstream cavities :

$$p'_{2,0} - p'_{1,L_1} = i\omega\rho_1 l\left(1 + \frac{l_v}{r_p}(1+i)\right)\frac{u'_{1,L_1}}{\mathcal{P}} \tag{4}$$

As the perforated plate is thin with a high porosity, one expects that its influence on the acoustic field will be weak. The acoustic volume flow rate experiences a jump through the flame region :

$$S_2 u'_{2,0} - N S_p u'_p = \frac{\gamma - 1}{\rho_1 c_1^2}\dot{Q}' \tag{5}$$

where S_2 represents the confinement section surface area, γ is the heat capacity ratio and $\dot{Q}'$ the heat release rate fluctuation. The right hand side term of Eq. 5 can be expressed by taking into account the response of the flame to velocity fluctuations with a Flame Describing Function (FDF). This quantity is obtained with the setup presented in Fig. 3. The conical flames are subjected to harmonic oscillation of increasing fluctuation levels up to 51 % for a range of frequencies up to 1600 Hz. FDF measurements are plotted in Fig. 7 in terms of gain G and phase φ defined as :

$$\mathcal{F}(\omega_r, |u'_p|) = \frac{\dot{Q}'\Big/\overline{\dot{Q}}}{u'_p/\overline{u}_p} = G(\omega_r, |u'_p|)e^{i\varphi(\omega_r,|u'_p|)} \tag{6}$$

where $\overline{\dot{Q}}$ stands for the mean value of the heat release rate fluctuation and $\overline{u}_p$ the mean value of the velocity in one hole. The FDF depends on both the frequency ω_r and the fluctuation amplitude u'_p as shown in Fig. 7. When the amplitude increases, the gain G drops and the phase φ shifts confirming the nonlinear behavior of the flame. This is the key point of the nonlinear stability analysis. As shown in this figure, the FDF data are limited by the lack of efficiency from the loudspeaker at high frequency and amplitude. The forcing root mean square velocity level u'_{rms} is determined by a Fourier transform and U_{bulk} stands for the mean value of the velocity profile measured 0.7 mm above one hole by means of LDV. It is equal to U_{bulk}=3.1 m.s^{-1}. The normalized ratio between the fluctuation of OH* radical light intensity and the velocity yields the gain G and the phase φ of the flame response. The flame acts as a low pass filter with a significant overshoot for higher frequencies and low fluctuation amplitudes. This behavior is also noted by other authors [9–11]. The phase evolves in a quasi linear fashion with the frequency and is sensitive to the fluctuation level. With the aim of using these measures for stability analysis, data are interpolated and extrapolated in missing areas. Considering the right hand side of Eq. 5 and the FDF (Eq. 6), one can write :

$$\frac{\gamma-1}{\rho_1 c_1^2}\dot{Q}' = \frac{\gamma-1}{\rho_1 c_1^2}\frac{\dot{Q}'\Big/\overline{\dot{Q}}}{u'_p/\overline{u}_p}\frac{u'_p/\overline{u}_p}{1\Big/\overline{\dot{Q}}} \tag{7}$$

In the present study, air and methane are considered to be ideal gases yielding, $c_1 = \sqrt{\gamma r T_1}$, $\overline{\dot{Q}} = \dot{m}c_p(T_f - T_1)$, $c_p = \frac{\gamma r}{\gamma - 1}$, $\dot{m} = \rho_1 N S_p \overline{u}_p$, where r is the gas constant of the mixture, $\dot{m}$ the mixture mass flow rate in one hole, c_p the specific heat at constant pressure and T_f the adiabatic flame temperature. Combining Eqs. 5 to 7, the velocity relation of Eq. 3 and the ideal gas relations, one obtains an expression for the acoustic volume flow rate jump condition across the flame sheet depending on the FDF :

$$S_2 u'_{2,0} - S_1 u'_{1,L_1} = G e^{i\varphi} S_1 \left(\frac{T_f}{T_1} - 1\right) u'_{1,L_1} \tag{8}$$

The preceeding set of equations can be used to obtain the following linear system :

$$\begin{pmatrix} 1 & -1 & 0 & 0 \\ 0 & 0 & e^{ik_2L_2} & e^{-ik_2L_2} \\ \mathcal{A}_1 e^{ik_1L_1} & \mathcal{A}_2 e^{-ik_1L_1} & -1 & -1 \\ \mathcal{B} e^{ik_1L_1} & -\mathcal{B} e^{-ik_1L_1} & -1 & 1 \end{pmatrix} \begin{pmatrix} A_1^+ \\ A_1^- \\ A_2^+ \\ A_2^- \end{pmatrix} = 0 \tag{9}$$

where $\mathcal{A}_1$, $\mathcal{A}_2$ and $\mathcal{B}$ corresponds to :

$$\mathcal{A}_1 = 1 + \frac{i\omega l}{\mathcal{P} c_1}\left[1 + \frac{l_v}{r_p}(1+i)\right],\ \mathcal{A}_2 = 1 - \frac{i\omega l}{\mathcal{P} c_1}\left[1 + \frac{l_v}{r_p}(1+i)\right],$$

$$\mathcal{B} = \frac{S_1}{S_2}\frac{\rho_2 c_2}{\rho_1 c_1}\left[1 + \left(\frac{T_f}{T_1} - 1\right)G e^{i\varphi}\right]$$

The determinant of this system must equal zero, to obtain non-trivial solutions. This condition provides the dispersion relation describing the dynamics of the system :

$$\begin{aligned} &\frac{S_1}{S_2}\frac{\rho_2 c_2}{\rho_1 c_1}\left[1 + \left(\frac{T_f}{T_1} - 1\right)G e^{i\varphi}\right]\sin(k_1L_1)\sin(k_2L_2) \\ &- \cos(k_1L_1)\cos(k_2L_2) + \frac{\omega l}{\mathcal{P} c_1}\left[1 + \frac{l_v}{r_p}(1+i)\right] \\ &\cos(k_2L_2)\sin(k_1L_1) = 0 \end{aligned} \tag{10}$$

The objective is to find complex roots $\omega = \omega_r + i\omega_i$ yielding oscillation frequencies $f = \omega_r/2\pi$ and growth rate ω_i of perturbations.

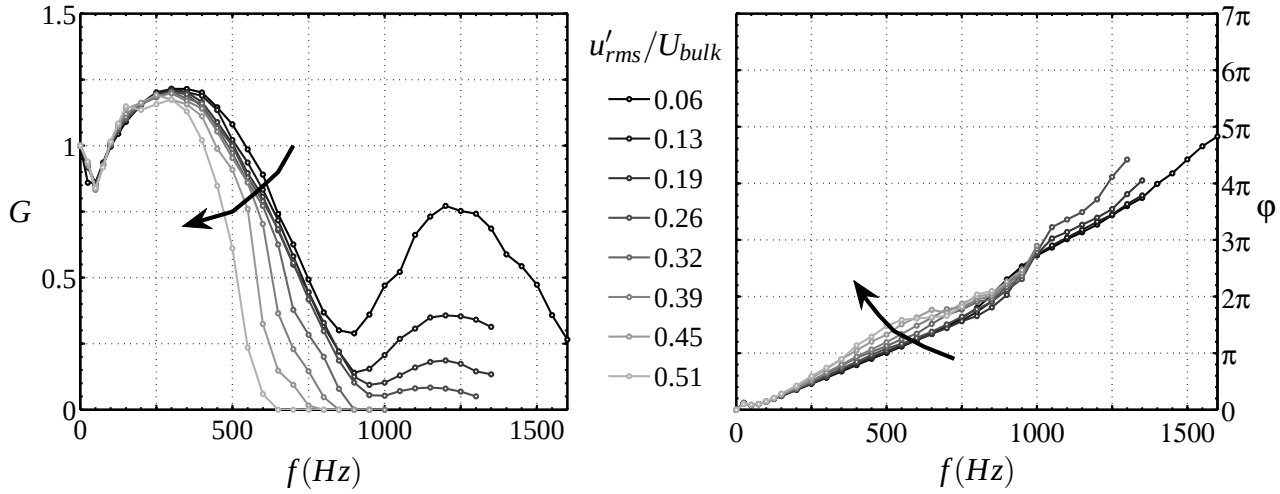

Figure 7. Experimental measurements of the Gain G and Phase φ of the FDF. u'_{rms} corresponds to the rms value of the fluctuation amplitude and U_{bulk} the mean flow velocity within one hole.

4 Theoretical and experimental comparison

The nonlinear analysis described in the previous section is now used to investigate the stability of the system. It is interesting to compare the experimental results from the self-sustained instabilities described in section 2 with the theoretical predictions of the oscillation frequencies and amplitudes at the limit cycle. Therefore, the FDF is used to calculate roots of the dispersion relation (10) for each driving amplitude. This yields ω_r and ω_i couples for each burner geometry and driving amplitude. For the differents lengths of feeding manifold and the L_2=10 cm confinement tube, calculations give the growth rate evolutions of the three first oscillation modes. Results are displayed in Fig. 8. This figure represents positive values of growth rate. Negative ones correspond to the white zone. Each color is dedicated to an oscillation mode; the first mode is drawn in yellow, the second in blue, and the third in red. Red dashed lines indicate the limit cycle corresponding to vanishing values of the growth rate.

From the different growth rate trajectories, it is possible to find, for each geometry, the evolution of the oscillation frequency of an instability up to the limit cycle. As presented in Fig. 8, the growth rates reveal three types of evolution. The first type of trajectory (for example dashed line "A" L_1=0.15 m) is positive for a small level of perturbation (u'_{rms}/U$_{bulk}$=0.1) and vanishes for a finite amplitude (0.6), and, as such, defines the limit cycle of the system. In this case, the system is linearly unstable. For the second type (for example dashed line "B" L_1=0.2 m), the growth rate of the first mode (yellow zone) is negative for small perturbation amplitudes but becomes positive at an amplitude of 0.3 and finally vanishes for a higher amplitude (0.65). This yields a limit cycle that can be triggered by a finite level of perturbation.

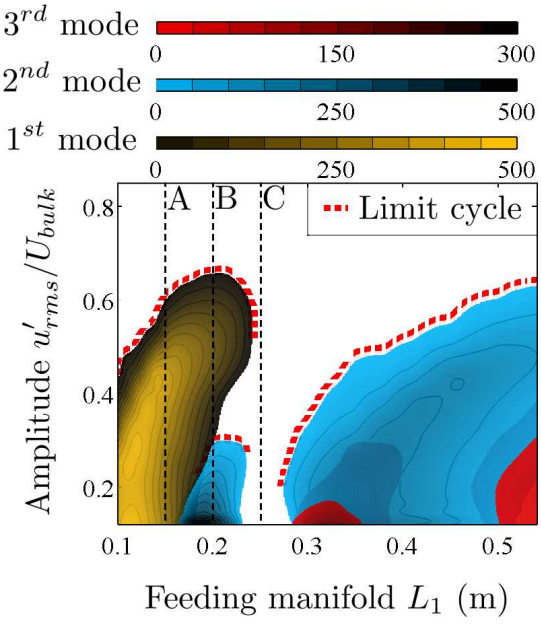

Figure 8. Positive values of the growth rate (in s^{-1}) for the 10 cm confinement as function of the length of the feeding manifold and the rate of fluctuation amplitude, u'$_{rms}$/U$_{bulk}$.

Indeed, a small level of perturbation cannot create an instability whereas a high oscillation level can. These limit cycles are nonlinearly unstable and linearly stable. The last type (for example dashed line "C" L_1=0.25 m) yields negative values of growth rate for all perturbation levels. In this case, the system is uncon-

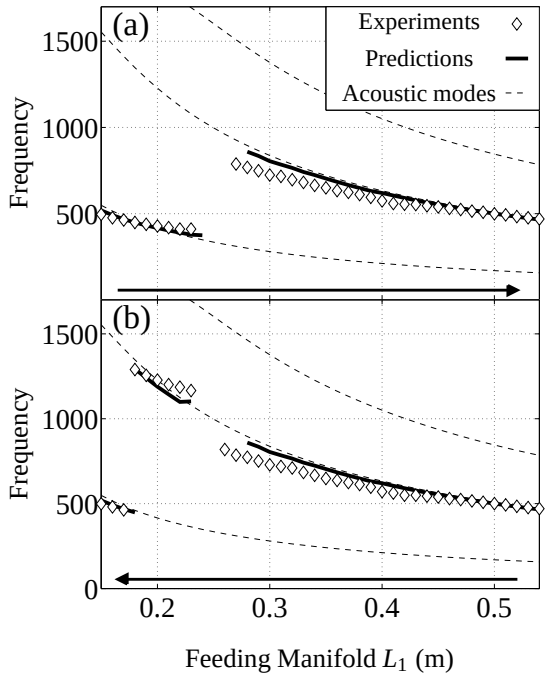

Figure 9. Experimental and predicted oscillation frequencies of self-sustained instabilities for the L_2=10 cm confinement tube for increasing (a) and decreasing (b) sweeps of the feeding manifold length L_1.

ditionally stable. Moreover, it can be deemed as both linearly and nonlinearly stable. In summary, it is found that the calculations show three types of growth rate evolution.

By analyzing the growth rate for each length of feeding manifold L_1 it is possible to find the limit cycle obtained when ω_i=0 and extract at the same time the oscillation frequency using the angular frequency ω_r. The limit cycle is reached when the growth rate is equal to zero. The acoustic damping δ is not taken into account in these calculations. For systems featuring large damping, limit cycles are reached when $\omega_i - \delta$=0. In the present case, the influence of δ is weak because growth rates take high values typically about 500 s^{-1} whereas δ in this system was estimated to be around 10 to 50 s^{-1} and does not significantly influence the results.

Figure 9 displays the evolution of the predicted oscillation frequencies and the experimental measurements. These predictions were obtained by analyzing the growth rate as detailed herein. In these figures, the acoustic eigenmodes, without flame (G=0 in the dispersion relation), are drawn as thin dashed lines. The frequencies predicted at the limit cycle using the nonlinear analysis are represented by bold lines and the experimental measurements are plotted as diamond signs. For each length of feeding manifold, (L_1), the frequency is extracted from the oscillations of the pressure signal (M_2). As presented in Fig. 4, for the L_2=10 cm confinement case there are two types of frequency evolutions. When the manifold length is increased (min to max) (Fig. 9a), the oscillation frequency evolves around the first eigenmode with a change around the second eigenmode after the stable zone between L_1=0.24 m and 0.26 m. In the reverse movement (max to min) (Fig. 9b), the frequency lies close to the second eigenmode until it becomes stable at L_1=0.26 m, but resumes around the second eigenmode for L_1=0.23 m to 0.18 m before it finally switches to the first mode for the last three lengths L_1=0.17 m to 0.15 m. This behavior, defined as an hysteresis, is well described by the growth rate analysis (see Fig. 8). When the piston is moved in the reverse direction (L_1 decreasing), the oscillation vanishes for three lengths of feeding manifold L_1=0.26, 0.25 and 0.24 m. After the stable zone, linearly unstable trajectories for the second mode yields a weak limit cycle between L_1=0.23 m and 0.18 m (blue zone). For shorter lengths $L_1 < 0.18$ m, the system is unstable on the first mode (yellow zone) as presented in Fig. 9b. At the beginning, when the manifold cavity was increased from L_1=0.15 m to 0.54 m, the system oscillates at high amplitudes for the first lengths L_1=0.15 m to 0.17 m. In this case, the instability stays on the first mode even if the growth rate trajectories of this mode become nonlinearly unstable between L_1=0.18 m and 0.23 m. The nonlinear impulse, needed to trigger the first mode, comes from the high oscillation amplitude reached at the previous length. The origin of this hysteresis is linked to the nonlinear behavior of the flame. Indeed, it is possible to predict the hysteresis by analyzing the FDF phase at the acoustic eigenmodes frequencies around the stable zone. If the phase of the FDF is comprised between π and 2π modulo 2π, the instability may develop [36, 43]. For the L_2=10 cm confinement case, when the instability evolves on the first mode at high amplitude (increasing L_1) the phase is in the right band between π and 2π (see Fig. 7) at L_1=0.23 m where f =400 Hz whereas this is not the case for the second mode f=1100 Hz. When the cavity length L_1 decreases, as the system leaves the stable zone at L_1=0.23 m, the phase for low oscillation amplitude lies in the right band for the high frequency f =1100 Hz of the second mode. This is the reason why the instability takes on second mode frequency values.

The growth rate evolution was also computed for the L_2=20 cm confinement tube and its reading yields the different limit cycle oscillation frequencies. These results are presented in Fig. 10. For this second confinement case, the evolution is simpler. When the feeding manifold length L_1 is increased, the instability frequency changes from the first mode between L_1=0.15 m to 0.25 m to the second mode between L_1=0.32 m to 0.54 m after a stable zone. When L_1 is decreased, the instability evolves in the same way. Thus, in this case, no hysteresis is observed. The theoretical analysis in terms of phase shows that the frequency of the second mode does not yield phase values in the right band at low or at high amplitude after the stable band at L_1=0.25 m. This is the reason why the system lies always on the first mode for perturba-

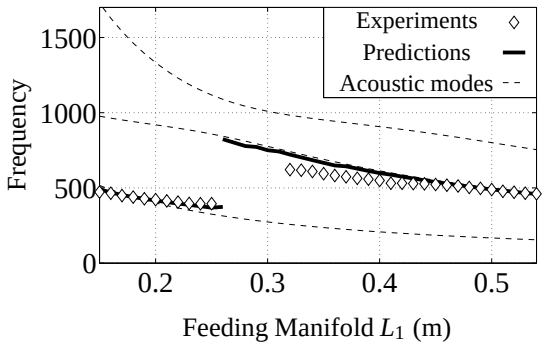

Figure 10. Experimental and predicted oscillation frequencies of self-sustained instabilities for the L_2=20 cm confinement tube. Increasing and decreasing L_1 has the same influence on the frequency evolution.

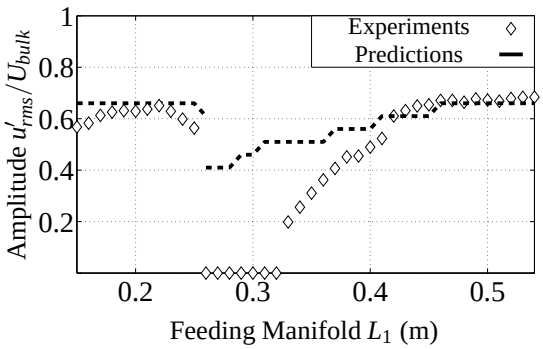

Figure 12. Experimental and predicted amplitudes of the instabilities for the L_2=20 cm confinement tube. Increasing and decreasing L_1 has the same influence on the amplitude evolution.

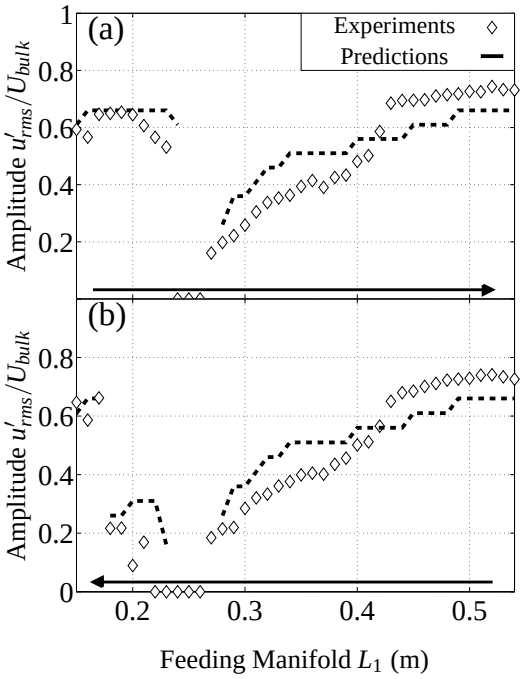

Figure 11. Experimental and predicted amplitudes of the instabilities for the L_2=10 cm confinement tube for increasing (a) and decreasing (b) sweeps of the feeding manifold length L_1.

tions at high or low amplitude. In this case, calculations are less reliable, as some oscillation frequencies are predicted in the stable zone. By analyzing the growth rate, it is shown that the model gives positive values for these lengths. These discrepancies can be linked to the accuracy of the FDF, showing the importance of getting the right flame response.

One advantage of the FDF methodology, is that, in addition to providing the limit cycle frequency, the growth rate analysis also predicts the amplitude. For each length of feeding manifold L_1 and each confinement tube length L_2, it is possible to find the oscillation amplitude when the instability oscillation is established. These results are presented in Fig. 11 for the L_2=10 cm confinement tube. The predictions are plotted as dashed lines whereas the experimental values, obtained by the hot wire probe, appear as diamond signs. Fig. 11a represents the evolution of the amplitude when L_1 is increased. The oscillation evolves at high amplitude for L_1 comprised between 0.15 m and 0.23 m. After the stable zone L_1=0.24, 0.25 and 0.26 m, the oscillation grows from a level around 0.19 to 0.7 for the longer feeding manifold length at L_1=0.54 m. By decreasing L_1, the oscillation evolves in the same way until the stable zone at L_1=0.26, 0.25 and 0.24 m. Then, the amplitude switches to a very low level around 0.1, or nearly close to zero for the hot wire values at L_1=0.23 m and 0.22 m. After L_1=0.18 m, the level increases abruptly to 0.7. The dashed line, which represents the results of calculations, is in good agreement with the levels measured in the expriments.

For the longer confinement tube L_2=0.2 m, the evolution is drawn in Fig. 12. In this case, the evolution is the same when the feeding manifold length L_1 is increased or decreased. From L_1=0.15 m to 0.25 m the amplitude lies around 0.6. It falls to 0 from L_1=0.26 m to 0.32 m. Then, the instability appears again with an increasing amplitude until it reaches 0.7 for the longer cavities. As one can see, predictions do not fully agree with measurements, indicating the influence of the FDF on the calculations and that some improvements need to be made in the FDF determination.

5 Conclusions

This work presents results of calculations of limit cycles based on the FDF framework for combustion instability analysis. The system studied herein is close to a real configuration in the sense that it features a feeding manifold that is used to

feed a multipoint injector and features a combustion region in a confined environment. The FDF, determined experimentally, exhibits nonlinearities of the flame response. This is used to derive a nonlinear dispersion relation providing predictions of the stable or unstable behavior of the combustor as a function of amplitude. Comparison with systematic experiments carried out by changing the feeding manifold length and flame tube size are in agreement with experiments over a broad range of parameters. Calculations are quite reliable in the case of a short flame tube but they are slightly off in the case of a longer tube where a difference is observed in a finite range of feeding manifold lengths. This may be corrected by improving the procedure to determine the FDF. It remains that the FDF analysis provides a suitable account of limit cycle amplitudes, hysteresis and mode switching observed in practice as demonstrated in the short flame tube case. Finally, it should be noted that linear analysis cannot provide reliable stability ranges of a system, because nonlinear triggering is possible in which a high amplitude disturbance exceeding a threshold may induce self sustained oscillations. This phenomenon is well retrieved from the growth rate trajectories determined from the FDF framework.

REFERENCES

[1] Lord Rayleigh, J., 1878. "The explanation of certain acoustical phenomena". *Notices of the proceedings members of the Royal Institution (of Great Britain),* ***3***, pp. 536–542.

[2] Crocco, L., and Cheng, S., 1956. *Theory of combustion instability in liquid propellant rocket motors*. AGARDOGRAPH number 8, Butterworths Science Publication.

[3] Putnam, A., 1971. *Combustion driven oscillations in industry*. Elsevier, New-York.

[4] Culick, F., 2001. *Dynamics of combustion systems : fundamentals, acoustics and control*. NASA.

[5] Candel, S., 2002. "Combustion dynamics and control: progress and challenges". *Proc. Comb. Inst.,* ***29***, pp. 1–28.

[6] Huang, Y., and Yang, V., 2009. "Dynamics and stability of lean-premixed swirl-stabilized combustion". *Progress in Energy and Combustion Science,* ***35***(4), pp. 293 – 364.

[7] Matsui, Y., 1981. "An experimental study on pyro-acoustic amplification of premixed laminar flames". *Combust. & Flame,* ***43***, pp. 199–209.

[8] Ducruix, S., Durox, D., and Candel, S., 2000. "Theoretical and experimental determination of the transfer function of a laminar premixed flame". *Proc. Combust. Inst.,* ***28***, pp. 765–773.

[9] Durox, D., Schuller, T., Noiray, N., and Candel, S., 2009. "Experimental analysis of nonlinear flame transfer functions for different flame geometries". *Proceedings of the Combustion Institute,* ***32***, pp. 1391–1398.

[10] Kornilov, V., Rook, R., ten Thije Boonkkamp, J., and de Goey, L., 2009. "Experimental and numerical investigation of the acoustic response of multi-slit bunsen burners". *Combustion and Flame,* ***156***(10), pp. 1957 – 1970.

[11] Schuller, T., Durox, D., and Candel, S., 2003. "A unified model for the prediction of laminar flame transfer functions : comparisons between conical and v-flame dynamics". *Combust. & Flame,* ***134***, pp. 21–34.

[12] Polifke, W., and Lawn, C., 2007. "On the low-frequency limit of flame transfer functions". *Combustion and Flame,* ***151***(3), pp. 437 – 451.

[13] Fleifil, M., Annaswamy, A., Ghoneim, Z., and Ghoniem, A., 1996. "Response of a laminar premixed flame to flow oscillations: a kinematic model and thermoacoustic instability results". *Combust. Flame,* ***106***, pp. 487–510.

[14] Schuller, T., Ducruix, S., Durox, D., and Candel, S., 2002. "Modeling tools for the prediction of premixed flame transfer function". *Proc. Combust. Inst.,* ***29***, pp. 107–113.

[15] Gentemann, A., Hirsch, C., Kunze, K., Kiesewetter, F., Sattelmayer, T., and Polifke, W., 2004. "Validation of flame transfer function reconstruction for perfectly premixed swirl flames". *ASME Conference Proceedings,* ***2004***(41669), pp. 501–510.

[16] Armitage, C. A., Riley, A. J., Cant, R. S., Dowling, A. P., and Stow, S. R., 2004. "Flame transfer function for swirled LPP combustion from experiments and CFD". *ASME Conference Proceedings,* ***2004***(41669), pp. 527–537.

[17] Truffin, K., and Poinsot, T., 2005. "Comparison and extension of methods for acoustic identification of burners". *Combustion and Flame,* ***142***(4), pp. 388–400.

[18] Giauque, A., Selle, L., Gicquel, L., Poinsot, T., Buechner, H., Kaufmann, P., and Krebs, W., 2005. "System identification of a large-scale swirled partially premixed combustor using LES and measurements". *Journal of Turbulence,* ***6***.

[19] Schuermans, B., Bellucci, V., and Paschereit, C. O., 2003. "Thermoacoustic modeling and control of multi burner combustion systems". *ASME Conference Proceedings,* ***2003***(36851), pp. 509–519.

[20] Poinsot, T., and Veynante, D., 2001. *Theoretical and Numerical Combustion*. Edwards, Philadelphia.

[21] Moeck, J., Oevermann, M., Klein, R., Paschereit, C., and Schmidt, H., 2009. "A two-way coupling for modeling thermoacoustic instabilities in a flat flame rijke tube". *Proceedings of the Combustion Institute,* ***32***(1), pp. 1199 – 1207.

[22] Krebs, W., Flohr, P., Prade, B., and Hoffmann, S., 2002. "Thermoacoustic stability chart for high-intensity gas turbine combustion systems". *Combustion Science and Technology,* ***174***(7), pp. 99–128.

[23] Paschereit, C. O., Schuermans, B., Polifke, W., and Mattson, O., 2002. "Measurement of transfer matrices and source terms of premixed flames". *Journal of Engineering for Gas Turbines and Power, ASME Trans.,* ***124***, pp. 239–247.

[24] Kim, K. T., Lee, J. G., Lee, H. J., Quay, B. D., and Santavicca, D., 2009. "Characterization of forced flame response of swirl-stabilized turbulent lean-premixed flames in a gas turbine combustor". *Proceedings of ASME Turbo Expo 2009*.

[25] Schuermans, B., Guethe, F., Pennel, D., Guyot, D., and Paschereit, C. O., 2009. "Thermoacoustic modelling of a gas turbine using transfer functions measured at full engine pressure". *Proceedings of ASME Turbo Expo 2009*.

[26] Martin, C., Benoit, L., Sommerer, Y., Nicoud, F., and Poinsot, T., 2006. "Large-eddy simulation and acoustic analysis of a swirled staged turbulent combustor". *AIAA Journal,* ***44***(4), pp. 741–750.

[27] Dowling, A., 1999. "A kinematic model of a ducted flame". *Journal of Fluid Mechanics,* ***394***(-1), pp. 51–72.

[28] Pankiewitz, C., and Sattelmayer, T., 2003. "Time domain simulation of combustion instabilities in annular combustors". *Journal of Engineering for Gas Turbines and Power,* ***125***(3), pp. 677–685.

[29] Bellows, B., and Lieuwen, T., 2004. "Nonlinear response of a premixed combustor for forced acoustic oscillations". In AIAA 2004-0455, AIAA, ed.

[30] Bellows, B., Zhang, Q., Neumeier, Y., Lieuwen, T., and Zinn, B., 2003. "Forced response studies of a premixed flame to flow disturbances in a gas turbine forced response studies of a premixed flame to flow disturbances in a gas turbine combustor". *41st Aerospace Sciences Meeting and Exhibit,* ***824***.

[31] Balachandran, R., Ayoola, B., Kaminski, C., Dowling, A., and Mastorakos, E., 2005. "Experimental investigation of the non linear response of turbulent premixed flames to imposed inlet velocity oscillations". *Combustion and Flame,* ***143***(1-2), pp. 37–55.

[32] Durox, D., Schuller, T., and Candel, S., 2005. "Combustion dynamics of inverted conical flames". *Proceedings of the Combustion Institute,* ***30***(2), pp. 1717 – 1724.

[33] Kim, D., Lee, J. G., Quay, B. D., Santavicca, D. A., Kim, K., and Srinivasan, S., 2010. "Effect of flame structure on the flame transfer function in a premixed gas turbine combustor". *Journal of Engineering for Gas Turbines and Power,* ***132***(2), p. 021502.

[34] Karimi, N., Brear, M. J., Jin, S.-H., and Monty, J. P., 2009. "Linear and non-linear forced response of a conical, ducted, laminar premixed flame". *Combustion and Flame,* ***156***(11), pp. 2201 – 2212.

[35] Noiray, N., Durox, D., Schuller, T., and Candel, S., 2008. "A unified framework for nonlinear combustion instability analysis based on the flame describing function". *Journal of Fluid Mechanics,* ***615***, pp. 139–167.

[36] Noiray, N., Durox, D., Schuller, T., and Candel, S., 2009. "A methof for estimating the noise level of unstable combustion based on the flame describing function". *International Journal of Aeroacoustics,* ***8***(1), pp. 157–176.

[37] Hield, P. A., Brear, M. J., and Jin, S. H., 2009. "Thermoacoustic limit cycles in a premixed laboratory combustor with open and choked exits". *Combustion and Flame,* ***156***(9), pp. 1683 – 1697.

[38] Staffelbach, G., Gicquel, L., Boudier, G., and Poinsot, T., 2009. "Large eddy simulation of self excited azimuthal modes in annular combustors". *Proceedings of the Combustion Institute,* ***32***(2), pp. 2909 – 2916.

[39] Hurle, I. R., Price, R. B., Sudgen, T. M., and Thomas, A., 1968. "Sound emission from open turbulent premixed flames". *Proc. Roy. Soc. A,* ***303***, pp. 409–427.

[40] Dowling, A. P., and Stow, S. R., 2003. "Acoustic analysis of gas turbine combustors". *J. Propuls. Power,* ***19***(5), Sep-Oct, pp. 751–764.

[41] Culick, F. E. C., 2006. *Unsteady motions in combustion chambers for propulsion systems.* AGARDograph, NATO/RTO-AG-AVT-039.

[42] Melling, T. H., 1973. "The acoustic impedance of perforates at medium and high sound pressure levels". *J. Sound & Vib.,* ***29***(1), pp. 1–65.

[43] Durox, D., Schuller, T., Noiray, N., Birbaud, A., and Candel, S., 2009. "Rayleigh criterion and acoustic energy balance in unconfined self-sustained oscillating flames". *Combustion and Flame,* ***156***, pp. 106–119.

ACKNOWLEDGMENT

This work was partially supported by the European FP7 project KIAI.